Published in final edited form as:

Clin Imaging. 2016 ; 40(1): 90–95. doi:10.1016/j.clinimag.2015.09.005.

Detection of Different Kidney Stone Types: An Ex-vivo Comparison of Ultrashort Echo Time MRI to Reference Standard CT

El-Sayed H. Ibrahim[a,b,*], **Joseph G. Cernigliaro**[a], **Robert A. Pooley**[a], **Mellena D. Bridges**[a], **Jamie G. Giesbrandt**[a], **James C. Williams**[c], and **William E. Haley**[a]

[a]Mayo Clinic, 4500 San Pablo Rd, Jacksonville, FL 32224, USA

[b]University of Michigan, 1500 E. Medical Center Dr, Ann Arbor, MI 48109, USA

[c]Indiana University, 340 W 10th St, Indianapolis, IN 46202, USA

Abstract

Background and Purpose—With the development of ultrashort echo time (UTE) sequences, it may now be possible to detect kidney stones by using magnetic resonance imaging (MRI). In this study, kidney stones of varying composition and sizes were imaged using both UTE MRI as well as the reference standard of computed tomography (CT), with different surrounding materials and scan setups.

Methods—One hundred and fourteen kidney stones were inserted into agarose and urine phantoms and imaged on both a dual-energy CT scanner using a standard renal stone imaging protocol and on an MRI scanner using the UTE sequence with both head and body surface coils. A subset of the stones representing all composition types and sizes was then inserted into the collecting system of porcine kidneys and imaged in vitro with both CT and MRI.

Results—All of the stones were visible on both CT and MRI imaging. Dual-energy CT was capable of differentiating between uric-acid and non-uric-acid stones. In MRI imaging, the choice of coil and large field-of-view did not affect stone detection or image quality. The MRI images showed good visualization of the stones' shapes, and the stones' dimensions measured from MRI were in good agreement with the actual values (R^2=0.886, 0.895, and 0.81 in the agarose phantom, urine phantom, and pig kidneys, respectively). The measured T2 relaxation times ranged from 4.2 to 7.5 ms but did not show significant differences among different stone composition types.

Conclusions—UTE MRI compared favorably with the reference standard CT for imaging stones of different composition types and sizes using body surface coil and large field-of-view, which suggests potential usefulness of UTE MRI in imaging kidney stones in vivo.

[*]Corresponding Author: Dr. El-Sayed Ibrahim, Department of Radiology, University of Michigan, 1500 E. Medical Center Dr. (UH-B2-A209), Ann Arbor, MI 48109, USA, Telephone: +1-734-615-8003, Fax: +1-734-764-2412, elsayei@umich.edu.

Conflicts of Interest: *None*

Keywords

MRI; Ultrashort echo time; Abdominal CT; Dual-energy computed tomography (DECT); Kidney stone imaging

1. INTRODUCTION

Kidney stone attacks are common. Most patients are young and middle-aged males who present with severe flank pain; however, there has been an increasing incidence of kidney stone attacks noted in women in recent decades. At least 50% of all such presentations involve radiological imaging [1]. After treatment of the acute attack, a large percentage of the patients have recurrent calculi, which may lead to chronic renal disease and other significant morbidities [2, 3].

Currently, computed tomography (CT) represents the gold standard for diagnostic imaging of kidney stones with almost 100% sensitivity and specificity [4]. The importance of the surrounding soft tissues for accurately measuring the attenuation coefficient of kidney stones in the resulting CT images has been confirmed in prior studies [5, 6]. The recent introduction of dual-energy CT (DECT) adds the capability of differentiating uric acid (UA) from non-UA stones with high sensitivity and accuracy (90%–100%) [7, 8]. DECT is an imaging technique that acquires two CT datasets at different energies, from which material-specific image can be formed by exploring the energy dependence of the attenuation coefficient for each tissue. While CT imaging of kidney stones has increased, concerns have been raised about the overuse of ionizing radiation in vulnerable patients, including young patients, pregnant women, and recurrent stone formers [9, 10]

MRI, which averts radiation concerns, is a potential alternative to CT imaging of kidney stones. However, the MR signal from the stones decays very rapidly, such that the echo times (TE's) used in conventional clinical imaging are not short enough to capture the signal before decaying. Therefore, stones appear as a dark non-specific signal void that may be confused with other tissues or image artifacts. With the advent of ultrashort echo time (UTE) MRI sequences, imaging of kidney stones has become possible [11]. The UTE sequence design allows for TE's in the range of tens of microseconds, which provides the opportunity for imaging tissues that have rapid signal decay, such as kidney stones.

In this work, we compare UTE MRI to DECT for imaging kidney stones of different stone composition types and sizes in phantom experiments using different surrounding materials and scan setups. We further investigate the capability of imaging different stone types inserted into pig kidneys using the abdomen/pelvis body surface coil, which is one step closer to in vivo MR imaging of kidney stones.

2. MATERIALS AND METHODS

2.1. Phantom Experiments

We utilized 114 kidney stones that had passed spontaneously or had been extracted from patients 1–5 years ago, the composition of which had been previously determined by micro-

CT analysis. The stone types and sizes are shown in Table 1. All stones were stored dry, at room temperature, in sealed containers to maintain stable mineral composition throughout the periods of observation [12]. Each of the 114 stone specimens used in this study was scanned by micro-CT using a Skyscan 1172 System (Bruker micro CT, Kontich, Belgium) with 60 kV X-ray source voltage and scanning/reconstruction settings to provide voxel size of 6–16 μm in the resulting 3D image stacks. This method for analyzing stones is unprecedented, allowing for the distinction of most of the major minerals within stones with microscopic spatial resolution [12, 13]. As shown in Figure 1, distinction of some minerals is obvious. In many common mineral combinations, micro-CT can detect minor minerals that occupy less than 1% of the volume of the stone, a detection limit that is not possible with spectroscopic analysis methods [14].

An agarose phantom (Figure 2(a,b)) was created as follows. One hundred and fourteen 5-ml tubes were filled with an agarose-based material, created by dissolving 0.5% agarose (Agarose Type 1, #6013; Sigma-Aldrich, St. Louis, MO, USA) in distilled water and doping the mixture with 0.085 milli-molar of $MnCl_2$ (Sigma-Aldrich, #416479) to create a gel-like material with T1 and T2 time constants similar to those in the kidney, as previously described [15]. The tubes were heated in a microwave for approximately two minutes for the agarose to completely dissolve in water. The tubes were then left to cool down so that the gel-like material solidified. Each kidney stone was inserted inside a separate tube when the agarose started to solidify.

The agarose phantom was imaged on a Siemens Flash DECT scanner (Siemens Healthcare, Forchheim, Germany) using renal stone imaging protocols with the following scan parameters: tube voltages/reference effective tube current-time product = 80 kVp/419 mAs and 140 kVp/162 mAs; collimation= 32×0.6 mm; and pitch= 0.7. Attenuation-based tube current modulation (CareDose 4D; Siemens Healthcare) was turned on. The images were post-processed to create material-specific chromatic image, based on the dual-energy ratio (DER) between the two images acquired with different kVp, with 1.0 mm slice thickness and using D30f convolution kernel.

2.2. UTE Imaging

Following the CT scan, the agarose phantom was imaged on a Siemens Skyra 3T MRI scanner (Siemens Healthcare, Erlangen, Germany) using a bird-cage head coil, which was large enough for the phantom to fit inside, as opposed to smaller wrist and knee coils. The point-wise encoding time reduction with radial acquisition (PETRA) 3D UTE pulse sequence was used for imaging the stones [16]. In the PETRA sequence, the outer k-space is filled with radial half-projections, where as the k-space center is measured point-wise on a Cartesian trajectory (Figure 3). The stones are imaged by acquiring two images with different TE's, which are subtracted to eliminate the signal from long-T2 tissues.

An initial scan session was dedicated to optimizing the imaging parameters for optimal visual results, including sufficient anatomical coverage (using dimensions that are large enough to cover the entire renal collecting system), high spatial resolution (submillimeter isotropic) to identify the smallest stones in the phantom without blurring, low background noise, and the shortest possible scan time. The optimized parameters were as follows: flip

angle = 6°; repetition time (TR) = 25 ms; first echo time (TE1) = 0.07 ms; second echo time (TE2) = 15 ms; resolution = 0.79×0.79 mm^3; slice thickness = 0.79 mm; field of view (FOV) = 280×280 mm^2; matrix = 352×352; number of slices = 352 (without gaps), number of radial spokes = 2500; bandwidth = 1895 Hz/pixel; number of averages = 1; and scan time = 3:21 min. Further technical notes: 1) Due to the intrinsically high signal-to-noise ratio (SNR) nature of 3D imaging, no additional averages or other pulse sequence modifications were needed to improve the signal, as is the case in typical high-resolution 2D imaging; 2) In previous experiments on smaller phantoms, we were able to achieve 65s scan time for covering a 150×150×150 mm^3 volume with 0.59 mm isotropic resolution. The stones were also imaged with different TEs ranging from 0.1 ms to 15 ms to measure their T2 time constants using exponential fitting with in-house software written in Matlab (The MathWorks Inc., Natick, MA).

The agarose phantom was then imaged again with MRI on the same scanner using the same protocol as described above, except that the head coil was replaced by an 18-channel body surface coil to examine scan-rescan reproducibility using the body surface coil, which is typically used for in vivo abdominal/pelvic imaging. After the second MRI scan, the stones were removed from the agarose-filled tubes, washed, and inserted in other tubes filled with urine to create a urine phantom, as shown in Figure 2(c). The urine phantom was then imaged with the same protocols and on the same scanners described above using only the body surface coil in MRI.

2.3. Pig Kidneys Imaging

A total of 24 kidney stones were selected from the 114 stones representing different stone types and sizes. A total of 8 pig kidneys, obtained from a local commercial market, were used in the experiments. Three stones (large, medium, and small) of the same composition type were inserted into different pig kidney calyces by way of small lateral incisions, which were then sutured after inserting the stone. Correct placement of the stones within calyces was confirmed following the scans (Figure 4(a)). A syringe was used to fill in the gaps around the stones inside the kidneys with water. The kidneys were then immersed into a plastic container filled with water, where they were pressed to remove air bubbles. The kidneys were stacked inside the container, which was then filled with water and closed with a sealed lid (Figure 4(b)). The kidneys were imaged on a Siemens Skyra 3T MRI scanner (Siemens Healthcare, Erlangen, Germany) using the MRI PETRA sequence as previously described in the phantom experiments.

2.4. Data Analysis

The images were evaluated by experts in MR and CT medical imaging (EI, RP, MB, JC). For each stone, the shape of the stone on the MRI images was visually compared with the actual stone shape for resemblance. Further, the maximum stone dimension was measured from the MRI images and compared with the actual value measured from the stone. Based on this data, student's *t*-test analyses were conducted to evaluate the significance of the size differences between the actual stone size and what was measured from the phantom and in vitro scans. A P-value < 0.05 was considered significant. Further, correlation and regression

analyses were conducted to evaluate the relationships between MRI measurements and actual measurements.

3. RESULTS

Scan time was 3:21 min for imaging the whole phantom (either agarose or urine) or the stack of pig kidneys in the plastic container. All stones were visible in the different CT and MRI phantom images, including all composition types and all size ranges. Dual-energy CT was capable of differentiating between UA and non-UA stones based on their dual-energy ratio (DER), where the UA and non-UA stones were shown red and blue, respectively, as illustrated in Figure 5.

The MRI image also showed all imaged stones with high resolution and details that reflect the actual stone shape, as shown in Figures 5 and 6. Using the body surface coil and large FOV did not affect the visibility of the stones, as comparable image quality was obtained from both head coil and body surface coil without increase in scan time.

Visual inspection revealed close resemblance between actual stone shapes and those observed on the MRI images. The statistical analysis showed close agreement between the stones' dimensions measured from the MRI images and actual values. There were no significant differences between the two sets of measurements based on student *t*-test statistical analysis results ($P = 0.995$, 0.606, and 0.197 for the measurements from the agarose phantom, urine phantom, and pig kidneys, respectively). The two sets of measurements showed good agreement, as demonstrated by the regression and correlation analyses results between the MRI measurements (Y) and actual measurements (X): $Y = 0.98X+0.059$ ($R^2 = 0.886$); $Y = 0.91X+0.11$ ($R^2 = 0.895$); and $Y = 0.97X-0.48$ ($R^2 = 0.81$) in the agarose phantom, urine phantom, and pig kidneys, respectively, compared with actual measurements.

MRI analysis of the stones showed T2 values that ranged from 4.2 to 7.5 ms in different stone types; however, there were no significant differences in the T2 measurements among the different stone types.

4. DISCUSSION

The results of the present study demonstrate the capability of UTE MRI for imaging kidney stones of different composition types and sizes with high resolution using a relatively short scan time. The images clearly and accurately showed the shapes of the stones and compared favorably with those obtained from the reference standard CT images and with measurements of the actual stones, irrespective of the receiver coil used for data acquisition or the material surrounding the stone. Further, we demonstrated that UTE MRI was successfully used for in vitro imaging of stones in pig kidneys using the body surface coil and large FOV, which is a step closer to in vivo MR imaging of kidney stones.

Kidney stone disease is a common and painful medical malady, and attacks frequently require imaging at initial presentation as well as at follow-up intervals to gauge treatment success. Accurate diagnosis is key to the prevention of serious complications [1–3]. CT has

emerged as the standard imaging modality with near 100% sensitivity and specificity [4], further enhanced by the introduction of dual-energy CT imaging [7, 8]. On the other hand, concerns regarding potential harm from radiation exposure have dampened enthusiasm for CT imaging, particularly in children, adolescents, and pregnant patients. MRI has proven useful in a number of conditions including the evaluation of kidney masses and liver disease. However, conventional MRI is insensitive to stone detection and has not been considered an adequate imaging modality for kidney stones due to rapid signal decay leading to nonspecific signal voids that are indistinguishable from other tissues or artifacts. The recent development of ultra-short echo time (UTE) sequencing with TE's in the microseconds has allowed for the possibility of imaging kidney stones with MR. However, the results of 2D UTE MRI of kidney stones have been disappointing [11].

Development of the point-wise encoding time reduction with radial acquisition (PETRA) 3D UTE pulse sequence [16] was found in the present study to be potentially useful for imaging kidney stones. In the PETRA sequence, the outer k-space is filled with radial half-projections, whereas the k-space center is measured point-wise on a Cartesian trajectory. Compared with conventional 2D UTE sequences [11], PETRA provides a much shorter TE over the whole k-space, which allows for better imaging of tissues with very short T2. The single-point imaging with T1 enhancement (SPRITE) approach used in the implemented 3D UTE PETRA in the present work resolves the limitations associated with conventional 2D UTE sequences by removing the delays associated with rapid gradient switching by turning on the imaging gradients prior to excitation [17]. Further, PETRA uses short RF pulses with wide bandwidth to equally excite the whole volume regardless of the imaging gradient strength. In addition, PETRA is less sensitive to eddy currents and gradient time delays than conventional 2D UTE sequences. Finally, the volumetric coverage provided by the 3D UTE sequence allows for scanning the whole volume of interest with high spatial resolution in much less time compared with 2D scans.

In our study, the whole volume of interest (280×280×280 mm^3) was covered at a resolution of 0.79 mm isotropic in 3:21 min (total of 352 slices, each has a matrix of 352×352). In contrast, the 2D UTE sequence used by Yassin et al [11] lasted for 5:32 min to acquire a single slice of 6 cm FOV. Further, four averages had to be acquired with the 2D UTE sequence to double SNR. Using the 3D UTE sequence in our study, only one set of data was acquired (# averages = 1) due to the high SNR intrinsic to 3D imaging. It is worth emphasizing that the current scan time of 3:21 min covers a 3D volume of 280×280×280 mm^3, which fits the cubical nature of the phantom. For in vivo scans, this volume is expected to be reduced, especially in the anterior-posterior and superior-inferior directions, with an associated reduction in scan time. So, a total scan time of under 2 min is expected for in vivo scans, during which high-quality images should be achievable, especially if the patient is asked to breathe shallowly and slowly during this short scan time. Nevertheless, our next step with in vivo scans will investigate this point in more detail to confirm this postulate or provide solutions in case of unexpected image artifacts.

A unique feature of the present study is the use of micro-CT for the determination of stone mineral content in the specimens used for study. This method is able to distinguish most stone minerals by their X-ray attenuation values in a completely nondestructive manner [14].

Thus each stone in the present study was either verified to be of pure composition, or the volume fractions of mixed minerals could be measured on the 3D image stack using simple segmentation techniques [18]. Because most urinary stones are of mixed mineral composition [19], other studies that have used “pure” stones are unlikely to have known whether some of their specimens may actually have been composed of more than one mineral.

The measured T2 relaxation values did not provide significant differences among different stone types using the described MRI technique. In contrast, the dual-energy CT imaging that was utilized in this study successfully differentiated between UA and non-UA stones. The inability of this MRI technique to distinguish between these categories of stone type represents a significant limitation compared with the gold standard DECT imaging of kidney stones. On the other hand, concerns that have been brought up about radiation exposure with CT scans [10] are averted with the MRI technique, making it a useful alternative to CT imaging, especially in patients who may be vulnerable to ionizing radiation. In addition, future work, including the investigation of other stone characteristics (e.g. morphology and surface topology) may be helpful to identify stone type using a multiparametric approach. A major limitation of the current study is the lack of in vivo results; nevertheless, the technique developed in this study and the seen couraging results from the phantom and in vitro experiments using the surface body coil and large FOV bring us closer to conducting in vivo experiments, which is our next step for future work.

The promising results in this work suggest the possibility of in vivo kidney stone imaging with UTE MRI, which, if successful, would be a valuable alternative to the reference standard DECT in patients at higher risk for radiation exposure, including children, adolescents, pregnant women, those of child-bearing potential, and recurrent stone formers. We envision that UTE MRI could also be added to other abdomen/pelvis MRI protocols for more comprehensive evaluation of the genitourinary system.

5. CONCLUSIONS

UTE MRI is capable of imaging kidney stones of the major different compositions and also of the spectrum of sizes between 2 and 10 mm with high resolution using a relatively short scan time. The images clearly and accurately showed the shapes of the stones and compared favorably with those obtained from the reference standard CT images, irrespective of the receiver coil used for data acquisition or the material surrounding the stone. Further, we demonstrated that UTE MRI was successfully used for in vitro imaging of stones in pig kidneys using the body surface coil ad large FOV, which is a step closer to vivo MRI imaging of kidney stone.

References

1. Coe FL, Evan A, Worcester E. Kidney stone disease. The Journal of clinical investigation. 2005; 115(10):2598–608. [PubMed: 16200192]
2. Romero V, Akpinar H, Assimos DG. Kidney stones: a global picture of prevalence, incidence, and associated risk factors. Rev Urol. 2010; 12(2–3):e86–96. [PubMed: 20811557]

3. Worcester EM, Coe FL. Clinical practice. Calcium kidney stones. N Engl J Med. 2010; 363(10): 954–63. [PubMed: 20818905]

4. Boulay I, Holtz P, Foley WD, White B, Begun FP. Ureteral calculi: diagnostic efficacy of helical CT and implications for treatment of patients. AJR Am J Roentgenol. 1999; 172(6):1485–90. [PubMed: 10350277]

5. Deveci S, Coskun M, Tekin MI, Peskircioglu L, Tarhan NC, Ozkardes H. Spiral computed tomography: role in determination of chemical compositions of pure and mixed urinary stones--an in vitro study. Urology. 2004; 64(2):237–40. [PubMed: 15302469]

6. Boll DT, Patil NA, Paulson EK, et al. Renal stone assessment with dual-energy multidetector CT and advanced postprocessing techniques: improved characterization of renal stone composition--pilot study. Radiology. 2009; 250(3):813–20. [PubMed: 19244048]

7. Primak AN, Fletcher JG, Vrtiska TJ, et al. Noninvasive differentiation of uric acid versus non-uric acid kidney stones using dual-energy CT. Acad Radiol. 2007; 14(12):1441–7. [PubMed: 18035274]

8. Matlaga BR, Kawamoto S, Fishman E. Dual source computed tomography: a novel technique to determine stone composition. Urology. 2008; 72(5):1164–8. [PubMed: 18619656]

9. Kalb B, Sharma P, Salman K, Ogan K, Pattaras JG, Martin DR. Acute abdominal pain: is there a potential role for MRI in the setting of the emergency department in a patient with renal calculi? J Magn Reson Imaging. 2010; 32(5):1012–23. [PubMed: 21031504]

10. Smith-Bindman R, Aubin C, Bailitz J, et al. Ultrasonography versus computed tomography for suspected nephrolithiasis. N Engl J Med. 2014; 371(12):1100–10. [PubMed: 25229916]

11. Yassin A, Pedrosa I, Kearney M, Genega E, Rofsky NM, Lenkinski RE. In vitro MR imaging of renal stones with an ultra-short echo time magnetic resonance imaging sequence. Acad Radiol. 2012; 19(12):1566–72. [PubMed: 22959582]

12. Williams JC Jr, McAteer JA, Evan AP, Lingeman JE. Micro-computed tomography for analysis of urinary calculi. Urological research. 2010; 38(6):477–84. [PubMed: 20967434]

13. Williams JC Jr, Sacks AJ, Englert K, et al. Stability of the infection marker struvite in urinary stone samples. Journal of endourology/Endourological Society. 2012; 26(6):726–31.

14. Zarse CA, McAteer JA, Sommer AJ, et al. Nondestructive analysis of urinary calculi using micro computed tomography. BMC urology. 2004; 4(1):15. [PubMed: 15596006]

15. Ibrahim el SH, Rana FN, Johnson KR, White RD. Assessment of cardiac iron deposition in sickle cell disease using 3.0 Tesla cardiovascular magnetic resonance. Hemoglobin. 2012; 36(4):343–61. [PubMed: 22563880]

16. Grodzki DM, Jakob PM, Heismann B. Ultrashort echo time imaging using pointwise encoding time reduction with radial acquisition (PETRA). Magn Reson Med. 2012; 67(2):510–8. [PubMed: 21721039]

17. Balcom BJ, Macgregor RP, Beyea SD, Green DP, Armstrong RL, Bremner TW. Single-Point Ramped Imaging with T1 Enhancement (SPRITE). J Magn Reson A. 1996; 123(1):131–4. [PubMed: 8980075]

18. Pramanik R, Asplin JR, Jackson ME, Williams JC Jr. Protein content of human apatite and brushite kidney stones: significant correlation with morphologic measures. Urological research. 2008; 36(5):251–8. [PubMed: 18779958]

19. Daudon M, Donsimoni R, Hennequin C, et al. Sex- and age-related composition of 10 617 calculi analyzed by infrared spectroscopy. Urological research. 1995; 23(5):319–26. [PubMed: 8839389]

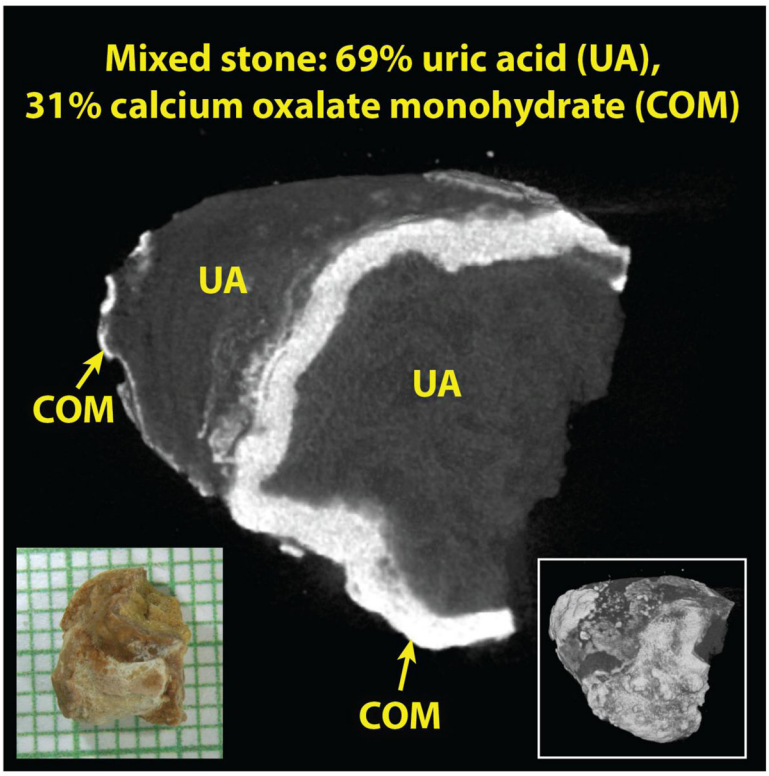

Figure 1.

Micro-CT slice through mixed uric acid and calcium oxalate stone. Note that uric acid has a much lower X-ray attenuation value than does calcium oxalate, so these two minerals are easily distinguished by micro-CT. Volume percentages of the two minerals was measured using simple segmentation of the 3D image stack. Lower left inset shows photo of stone on mm-grid paper. Lower right shows surface rendering of stone in the same orientation as the image slice.

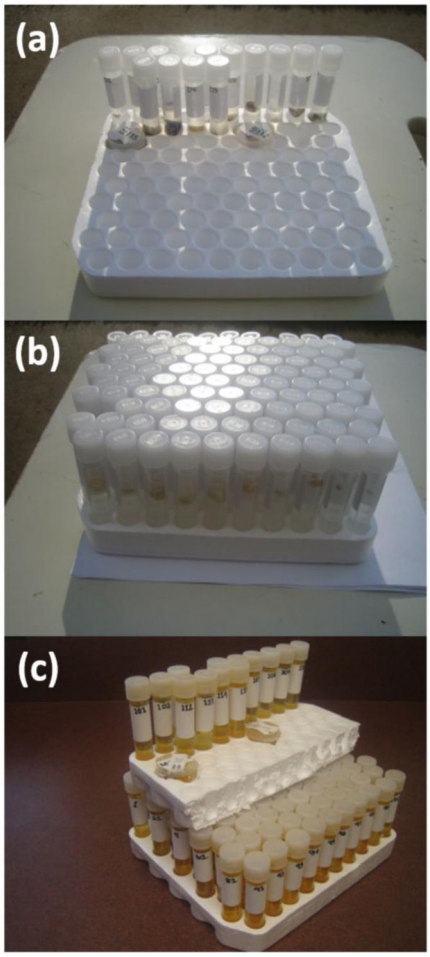

Figure 2.
Agarose phantom (a,b), and urine phantom (c).

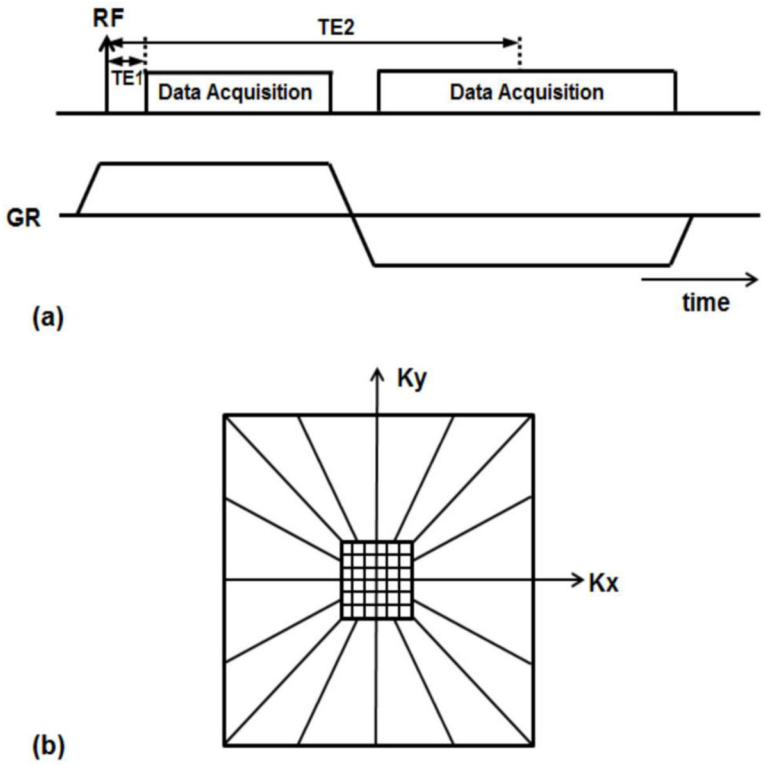

Figure 3.
UTE PETRA pulse sequence.(a) Radial acquisition of k-space periphery, where the gradients are ramped before RF excitation. (b) k-space sampling, where the k-space center is acquired in Cartesian fashion.

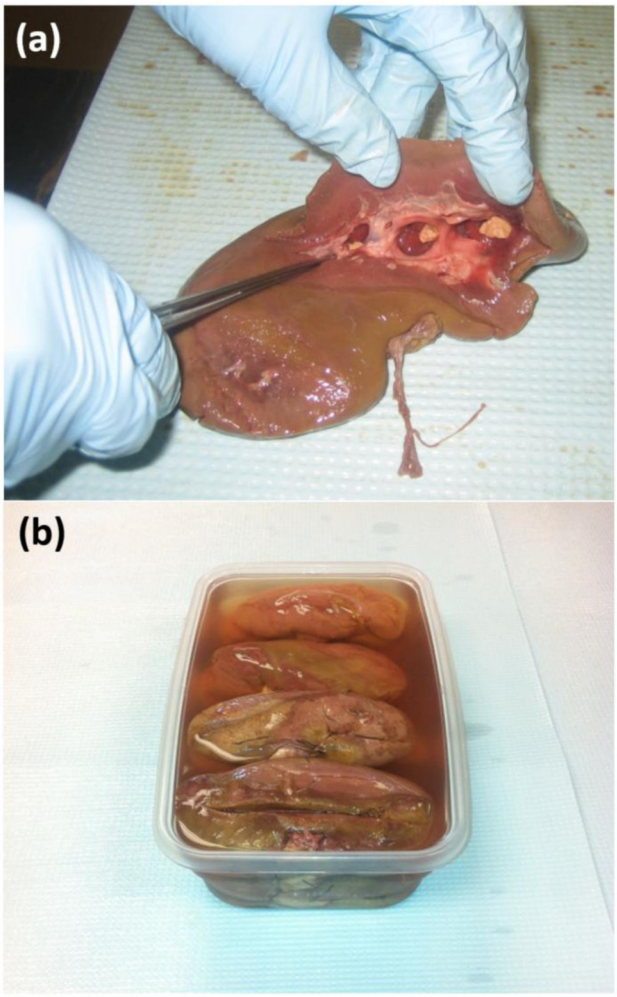

Figure 4.

Kidney preparation. (a) Three stones of the same type, but with different sizes (small, medium, and large), were inserted into different calyces of each pig kidney. The stones are inserted inside the calyces via small incisions, which were sutured afterwards to avoid stone movement. This picture was taken after the MRI scan to show stones positions. (b) Different kidneys were stacked in a plastic bin, which was then filled with water and covered with a sealed lid.

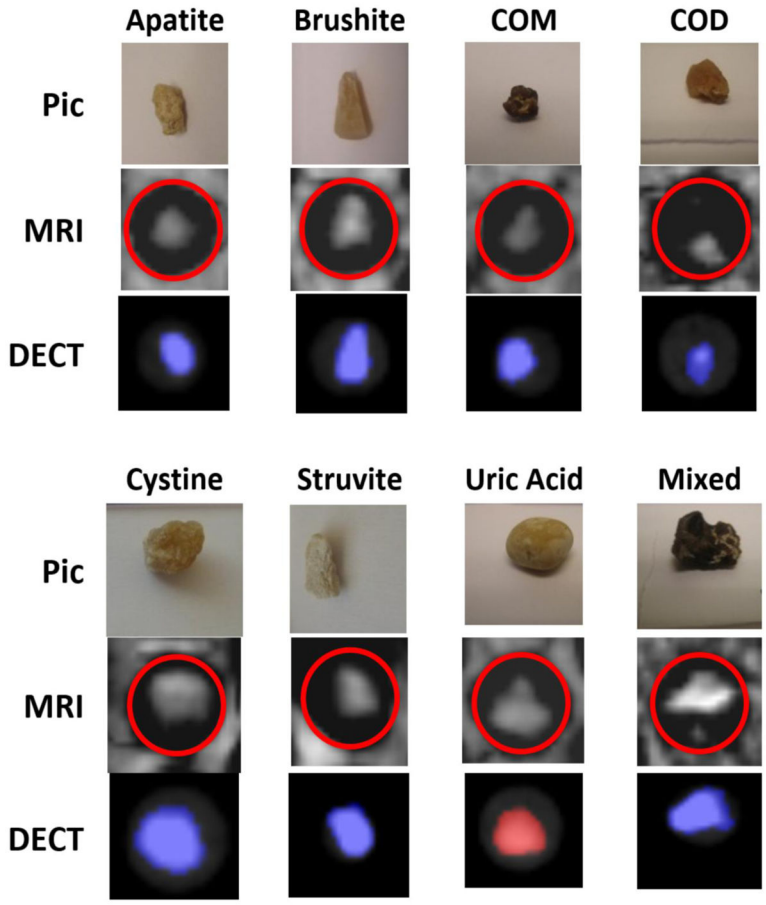

Figure 5.
Different stones (top) imaged with UTE MRI (middle) and DECT (bottom) in the phantom experiment. Pic, photograph of stones; COM, calcium oxalate monohydrate; COD, calcium oxalate dihydrate.

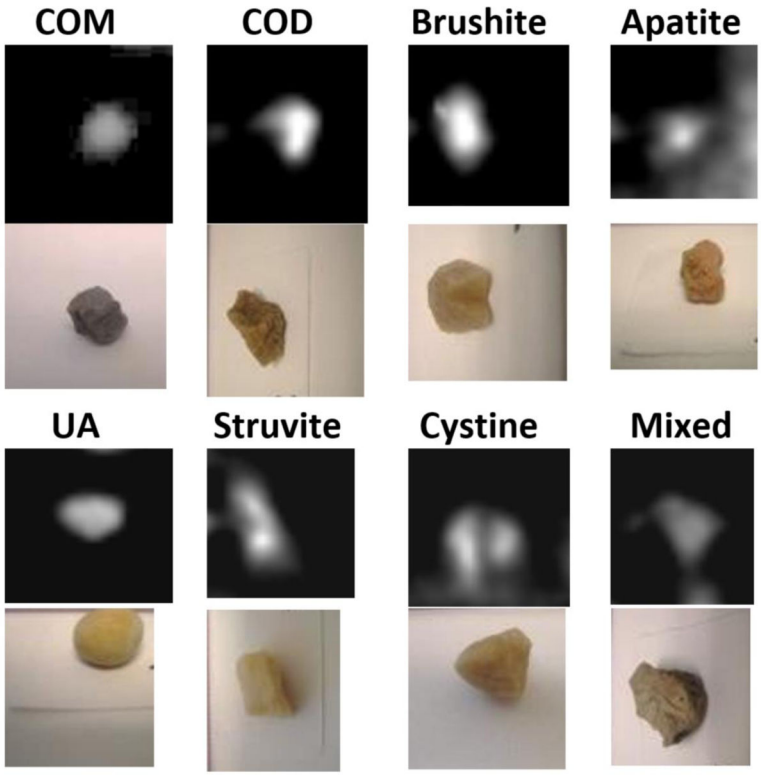

Figure 6.
Different kidney stones imaged with MRI using a body surface coil in the pig kidney scan, and photographs of the actual stones below each.

Table 1

Stones types and size*

Type	Apatite			Brushite			COD			COM		
Size	sm	md	lg	sm	md	lg	sm	md	lg	sm	md	lg
#	6	4	5	4	6	5	4	7	4	5	6	4
Type	**Cystine**			**Struvite**			**UA**			**Mixed**		
Size	sm	md	lg	sm	md	lg	sm	md	lg	sm	md	lg
#	2	7	7	1	7	7	5	4	6	0	0	8

*sm, small (2–3 mm); md, medium (4–6 mm); lg, large (7–10 mm).

Clin Imaging. Author manuscript; available in PMC 2017 June 27.